J. Fluid Mech. (2006), *vol.* 553, *pp.* 119–141.
doi:10.1017/S0022112006008986 Printed in the United Kingdom

Wakes and vortex streets generated by translating force and force doublet: laboratory experiments

By Y. D. AFANASYEV AND V. N. KORABEL

Memorial University of Newfoundland, Department of Physics and Physical Oceanography, St John's, NL, Canada, A1B 3X7
yakov@physics.mun.ca

(Received 8 November 2004 and in revised form 26 October 2005)

Wakes and vortex streets such as those occurring behind towed or self-propelled bodies are generated by moving localized forces in a viscous fluid at moderate values of the Reynolds number, $Re \sim 10^2$. The forcing is provided by an electromagnetic method and allows us to create a 'virtual' body without introducing any solid objects into the fluid. Characteristics of stable and unstable wakes, in particular the shedding frequency, are measured in the space of control parameters, namely the magnitude of the forcing and the speed of translational motion of the forcing. The results for a single force presented in the dimensionless form of the Strouhal number demonstrate quantitative similarity to those for the classical flow around a cylinder. The problem considered here has an extra degree of freedom compared to the problem of the flow around a cylinder and exhibit a wider array of different regimes. These regimes are documented in both our visualization experiments and particle image velocimetry measurements.

1. Introduction

A solid body moving in a viscous fluid generates a vortical wake which often becomes unstable. The instability results in the development of a regular array of vortices of alternating sign in the wake. A quantitative description of an unstable wake presents a difficult problem even if the shape of the body is relatively simple such as a cylinder. The flow around a cylinder is a classical problem in fluid mechanics and has a long history of serious investigation (see comprehensive reviews by Zdravkovich 1997 and Williamson & Govardhan 2004). The problem of the flow around a cylinder belongs to a wider class of problems which consider a bluff body towed in a fluid. A towed object experiences a drag force. The effect of the object on the fluid is therefore described by the force equal to the drag force in magnitude and acting in the opposite direction. A continuous transfer of momentum to the fluid takes place when the body is towed. In contrast, self-propelled bodies such as swimming micro-organisms or submarines, generate zero-momentum flow when moving with constant speed because they have to transfer momentum to the fluid in the direction opposite to that of their motion to generate the thrust force. If a self-propelled body moves with constant speed, the drag and thrust forces are of equal magnitude and of opposite directions. The drag force is applied near the front of the body while the thrust force is usually generated near the rear end. Thus, these forces are separated by a distance which is approximately equal to the length of the body. The same is also valid for

the corresponding reaction forces which act on the fluid. Herein, we formulate an idealized problem where the effect of the moving objects is effectively reduced to a combination of spatially localized forces acting on the fluid. The flows sufficiently far from the object (far-field flow), where the effect of the details of the shape of the body are negligible, are asymptotically similar to that generated by localized forces. In the near-field, the details of the distribution of forcing are important. We will show in particular that the finite size of the area where the force is applied is an important control parameter when the shedding of vorticity is concerned. A similar approach with localized forcing was realized in the experiments by Voropayev *et al.* (2002) and Voropayev & Smirnov (2003) where the source of forcing was a jet ejected from a nozzle horizontally in a stratified fluid. The nozzle was translated horizontally in the fluid in their experiments. Here we chose a different experimental method, namely electromagnetic forcing, which allows us to generate flows without inserting any solid objects into the fluid. It also provides greater flexibility in experiments where two forces of equal magnitude must be created. Our experiments are performed in a thin layer of stratified fluid which was demonstrated (e.g. Afanasyev & Korabel 2004) to work well in simulating the (quasi) two-dimensional flows.

If a single force starts acting in an initially quiescent viscous fluid, a starting vortex dipole is generated. A combination of two forces of equal magnitude but of opposite direction (force doublet) generates a vortex quadrupole consisting of two dipoles propagating in opposite directions. These prototype flows in stratified fluid or in a thin layer of fluid (quasi-two-dimensional) have been investigated by, for example, Voropayev & Afanasyev (1994) and Afanasyev & Korabel (2004). If a single force or a force doublet moves with constant speed in a fluid, it generates a wake with a vorticity distribution similar to that generated by stationary forcing, but rather stretched along the x-axis by the oncoming stream. A theoretical solution which describes the vorticity and streamfunction in both two-dimensional and three-dimensional (axisymmetric) flows generated by a point force or a force doublet were obtained in Afanasyev (2004) in the Oseen approximation.

In the following sections of this paper we report the results of laboratory experiments investigating different regimes of the flow generated by a moving localized forcing. The experimental apparatus, an electromagnetic method that allows us to model the motion of a virtual body in a thin layer of fluid, the calibration of the forcing and the methods of visualization and particle image velocimetry (PIV) are described in § 2. The results of the visualizations as well as the results and interpretation of measurements of the flow characteristics, in particular the vortex-shedding frequency for different values of the control parameters of the flow, are discussed in § 3. Discussion and concluding remarks are offered in § 4.

2. Experimental technique

The laboratory experiments reported herein were conducted in a long rectangular tank which is 120 cm long, 10 cm deep and 30 cm wide (figure 1). The tank was filled with two layers of salt water of height 0.5 cm each and of concentration 30 and 250 g l^{-1}. The flow was forced electromagnetically by imposing an electric current of magnitude $j = 0$–6 A in the horizontal direction. One or two rare earth permanent magnets of diameter 0.5 cm were located approximately 0.1 cm above the surface of water. The magnets were translated along the tank by a carriage driven by a computer-controlled stepping motor on a translating stage. The translation velocity was varied in the range $U = 0.15$–2.4 cm s^{-1}. Each magnet produces a magnetic field

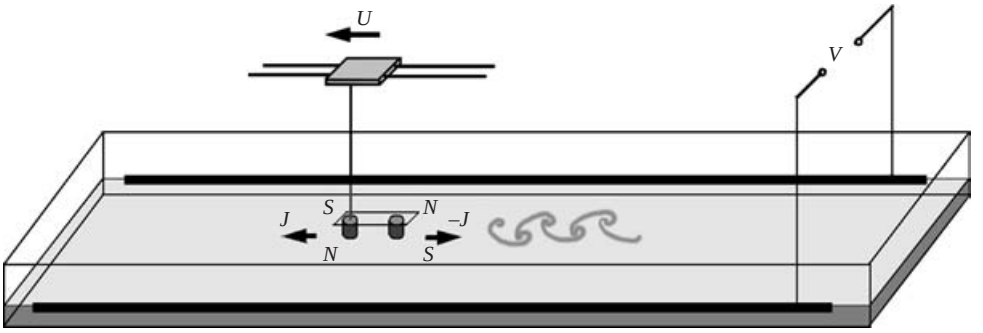

FIGURE 1. Sketch of the experimental set-up.

with a vertical component of approximately 0.09 T. The interaction of the magnetic field with the electric current results in a horizontal force exerted locally on the fluid in the direction perpendicular to the electric current. Charged particles (ions in dissociated electrolyte solution) moving in a magnetic field $\boldsymbol{B}$ experience the Lorentz force $\boldsymbol{F} = q\boldsymbol{v} \times \boldsymbol{B}$, where q is the charge and $\boldsymbol{v}$ is the velocity of a particle. The particles drift towards the electrodes such that positive ions move towards the cathode while negative ions move towards the anode. The Lorentz force is perpendicular to both the magnetic field and the current (drift velocity $\boldsymbol{v}$). Since the oppositely charged particles move in opposite directions the resulting force is in the same direction in the horizontal plane for positive and negative ions. If on the other hand, the particles in addition to drift are carried by the fluid motion, the total force due to this additional velocity component is zero since positive and negative particles move in the same direction and their total charge is zero. Thus the electromagnetic force on the fluid does not depend on the motion of the fluid. The force is applied locally to the fluid in a volume where the vertical component of the magnetic field is significant. To characterize the shape of this volume consider a magnetic field induced by a permanent magnet of cylindrical form. Assume that magnetization $\boldsymbol{M}$ of the magnet is uniform over its volume and is directed along the z-axis. The magnetic field induced by and elementary magnetic (dipolar) moment $\boldsymbol{m}$ is given by

$$\boldsymbol{B}(\boldsymbol{R}) = \frac{3\boldsymbol{n}(\boldsymbol{nm}) - \boldsymbol{m}}{R^3}, \tag{2.1}$$

where $\boldsymbol{R}$ is the position vector of a point where the magnetic field is measured and $\boldsymbol{n}$ is the unit vector in the direction of $\boldsymbol{R}$. The vertical component of the magnetic field induced by a cylindrical domain can be obtained easily by integration over the volume:

$$B_z = M \int_{-h}^{0} \int_{0}^{a} \int_{0}^{2\pi} \frac{3(z-z') - ((z-z')^2 + r^2 + r'^2 - 2rr'\cos(\varphi - \varphi'))^{1/2}}{((z-z')^2 + r^2 + r'^2 - 2rr'\cos(\varphi - \varphi'))^2} \, \mathrm{d}z' r' \, \mathrm{d}r' \, \mathrm{d}\varphi', \tag{2.2}$$

where h is the height and a is the radius of the magnet. Integration is performed in cylindrical polar coordinates (r, φ, z). Isosurfaces of B_z calculated from (2.2) are depicted in figure 2. Assuming that the magnet is at a distance 0.1 cm from the surface of the water, the maximum value of the magnetic field in the fluid will be at the surface along the symmetry axis of the magnet ($r = 0$, $z = 0.1$ cm) and will decay further away from the magnet. The surfaces which enclose the values of B_z exceeding 50 % or 20 % of the maximum value are depicted in figure 2. The size of the volume where

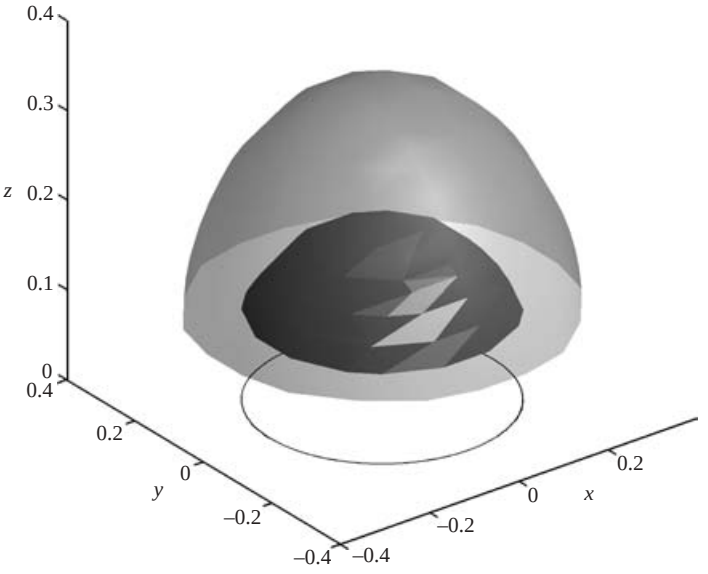

FIGURE 2. Isosurfaces of the magnetic field induced by a cylindrical magnet located at a distance of 0.1 cm from the surface of water. The isosurfaces show 50 % and 20 % of the maximum value of the magnetic field. The circle in the (x, y)-plane indicates the location of the magnet.

magnetic field is significant is of the order of the diameter ($d = 2a$) of the magnet in the horizontal direction and approximately half of that distance in the vertical direction. Thus the magnet only induces motion of the fluid in the upper layer. Without exact knowledge of drift velocities of ions in the fluid it is impossible to estimate the exact value of the force acting in the fluid. However, we can use an indirect method to obtain the value of this important control parameter. The magnitude of the force is controlled in the experiments by varying the current. If a magnet is stationary, the localized force generates a starting vortex dipole. Our previous results (Afanasyev & Korabel 2004) predict that the distance travelled by a dipole varies with time as

$$L(t) = \left(\frac{3J}{4\pi}\right)^{1/3} t^{2/3}. \tag{2.3}$$

This allows us to relate the momentum per unit time per unit depth of the layer, J, to the magnitude of the electric current. We measured L as a function of time using video sequences documenting the development of dipoles for different values of current j. First, the power law (2/3) dependence was confirmed. The momentum flux J was then estimated from the value of the slope of the dependence L versus $t^{2/3}$. The linear relation between the control parameter J and the current j was found to have the form $J = \beta j$ where β is a coefficient which depends on the particular parameters of the apparatus (the distance of the magnet from the surface of water, the magnetization of the magnet, the area of the electrodes and the stratification). In most of the experiments where we used the same set-up, the value of this coefficient was in the range $\beta = 0.3$–1.5 for J measured in $\mathrm{cm}^3\,\mathrm{s}^{-2}$ and j in A. In the experiments with two magnets, the values of the coefficient for both magnets were close to each other within 4 % accuracy. In this calibration we assumed that the flow is approximately uniform in the vertical direction along the depth of the layer. Our observations of the flow visualized by dye show that this is a valid assumption. Although the fluid particles

Series	Experiment	J ($\mathrm{cm^3\,s^{-2}}$)	U ($\mathrm{cm\,s^{-1}}$)	Symbol
1	9	0.22–1.6	0.58	+
2	10	0.27–1.6	0.87	◇
3	5	0.54–1.6	1.16	*
4	8	0.54–1.6	1.45	□
5	5	0.8–1.6	1.74	○

TABLE 1. Experimental parameters for the experiments with a single magnet.

Series	Experiment	J ($\mathrm{cm^3\,s^{-2}}$)	U ($\mathrm{cm\,s^{-1}}$)
1	7	0.8–3.1	0.58
2	11	0.25–3.1	0.87
3	8	0.8–3.1	1.16
4	7	1.3–3.1	1.45
5	5	1.5–3.1	1.74

TABLE 2. Experimental parameters for the experiments with two magnets.

move somewhat faster at the surface than at the interface between the layers, the velocity shear is relatively small (and decreases with time owing to vertical diffusion of momentum) such that the difference between the horizontal displacements of particles travelling at different depths is small compared to the length scale of the flow. Note that in the experiments described in this paper we used magnets of relatively small size. The reason for this choice is that the relation (2.3) was obtained for the flow induced by a point force. It was demonstrated in Afanasyev & Korabel (2004) that this relation works well when the values of dimensionless parameter $\Pi_2 = Ja/\nu^2$ which characterizes the effect of the finite size of the magnet, are not very large. For larger magnets the calibration method described here will result in inaccurate values of J and a different method must be used for this purpose.

In the experiments with a single magnet, the polarity of the magnet and the direction of the current were chosen such that the resulting force was applied on the fluid in the same direction as that of the translation of the magnet. This imitates the force applied by a towed body on the fluid (a reaction to the drag force). In the experiments with two magnets (force doublet), the magnet in the rear acted in the opposite direction thus simulating the reaction to the thrust force applied by a self-propelled body. Since the drag and thrust forces were of the same magnitude (but of opposite directions) this system simulates a self-propelled body moving with constant speed. Parameters of the experiments with the single and the double forces are summarized in tables 1 and 2.

Two layers were used to minimize the vertical component of velocity, providing two-dimensionality of the flow. The process of two-dimensionalization of the flows in a thin two-layer system was studied in detail by Paret *et al.* (1997) who demonstrated that vortices effectively adjust such that they can be considered almost uniform in the vertical direction. The particular parameters of our system were the same as those used in our previous experiments with two-dimensional turbulence (Wells & Afanasyev 2004). This system was shown to work well in achieving this purpose. In particular, an important result of the study on two-dimensional turbulence was the growth of the Reynolds number of the flow which was in agreement with the predictions for the two-dimensional turbulence (e.g. Chasnov 1997). This growth was previously achieved

only for flows in soap films (Martin *et al.* 1998). This provides additional evidence of the two-dimensional dynamics of the flow. In a thin-layer system, bottom friction is an important factor which prevents the flow from being purely two-dimensional. Bottom friction, as well as friction due to ordinary viscosity, causes the total energy of the flow to decay (e.g. Paret *et al.* 1997; Danilov *et al.* 2002). It is important therefore to keep the rate of energy decrease due to bottom friction at somewhat less than that due to ordinary viscosity, such that this effect is not too restrictive. This was demonstrated to be the case in Wells & Afanasyev (2004). We assume that this is also true for the present experiments where the magnitude of forcing is similar to that used previously. A simple estimate of a characteristic time required for the bottom boundary layer to diffuse a certain distance can be obtained from a self-similar solution for the boundary layer on a flat plate $u = U\mathrm{erf}(\xi)$ (e.g. Batchelor 1967). Here, $\xi = z/2(\nu t)^{1/2}$ is the similarity variable which suggests an estimate for the characteristic time to be $t = z^2/4\nu$. Therefore, it takes 25 s to diffuse a distance of 1 cm and 6 s for a distance of 0.5 cm. The lowest value of frequency of vortex shedding observed in our experiments is approximately $f = 0.1\,\mathrm{s}^{-1}$ (the highest frequency $f = 0.4\,\mathrm{s}^{-1}$), which corresponds to a period of $T = 10$ s (lowest period $T = 2.5$ s). Thus we can reasonably assume that the 'internal oscillator' which is responsible for vortex shedding is not affected by the viscous boundary layer while being approximately uniform through the depth of the upper layer. The shed vortices form a wake which develops on the larger time scale and is therefore affected by the bottom effects. The system is therefore more dissipative for longer times if compared to deep-layer systems.

For the purpose of comparison of a thin-layer stratified system used here with experimental set-ups where a deep layer of homogeneous fluid and a long cylinder are used for the investigation of bluff-body wakes, it is important to estimate whether the generation of surface (gravity/capillary) or internal waves is important. To estimate the amplitudes of the perturbations at the surface or the interface, we must estimate the perturbations of pressure due to the unsteady nature of the flow. Taking the lowest period $T = 2.5$ s of oscillations observed in the experiments and the size, $2a$, of the region where the forcing is applied to be the time scale and the length scale of the flow, we can obtain the characteristic pressure perturbation $p = \rho(2a/T)^2$. The perturbations of pressure will cause perturbations of the surface of the order $\zeta = (2a/T)^2/g = 10^{-4}$–$10^{-5}$ cm. The magnitude of the perturbations at the surface is therefore extremely small and the effect of generation of any surface waves can be safely ignored. Besides, the typical velocity of the flow is much less than the phase speed of gravity/capillary waves ($c_p = 25\,\mathrm{cm\,s}^{-1}$ when the wavelength is $\lambda = 1$ cm) such that the corresponding Froude number is small. Note that since there is no solid body piercing the surface in our experiments, there are no perturbations of surface associated with the wetting effect. Thus a possible generation of capillary waves due to vibrations at acoustic frequency is not an issue in our experiments. On a related note, a streaming effect which includes the production of vorticity by a solid body vibrating in fluid is absent here. Note that this effect can be very important and even dominating under certain conditions for the flow around a solid body. Laboratory experiments where a very thin cylinder oscillated in a stream demonstrated the formation of a typical Kármán–Bénard vortex street (Afanasyev & Filippov 1995). In those experiments, the diameter of the cylinder was small such that the Reynolds number was less than critical. Therefore, there was no vortex shedding if the cylinder was stationary in the stream and the occurrence of the vortex street was only due to the vorticity generated by the streaming effect. Another effect which is worth discussing here is a finite extent of the forcing in the vertical direction. The

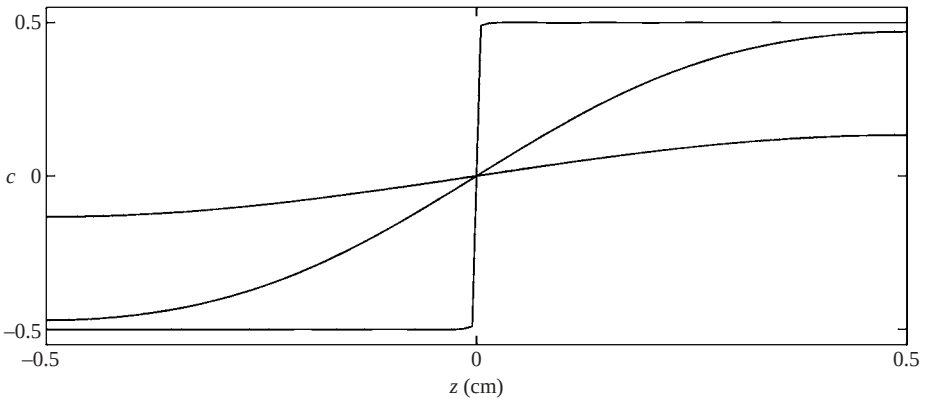

FIGURE 3. Vertical profiles of concentration for different times $t = 6$, 60 min. Step-like profile indicates the initial distribution.

experiments with finite cylinders demonstrate that a tip vortex of horseshoe form is created at the free end of the cylinder (e.g. Roh & Park 2003; Sumner, Heseltine & Dansereau 2004). For cylinders of small aspect ratio, the flow around the free end may affect the flow along the entire cylinder height such that the Kármán–Bénard vortex shedding can be suppressed. In our experiments, the forcing decayed gradually with depth in contrast to the case of the finite cylinder. In addition to that effect, strong density stratification effectively suppressed any three-dimensional perturbations such that no tip vortex was observed.

To estimate the effect of the generation of internal waves, we need to know the typical parameters of the stratification. The tank was filled very carefully to avoid any mixing. The filling process typically took 5–10 min. Assuming that diffusion starts immediately, we can estimate the evolution of the vertical density distribution in the system. Solving the equation of diffusion with no-flux boundary conditions at the surface and at the bottom and step-like initial distribution of concentration, we obtain by separation of variables:

$$c(z,t) = \sum_{n=1,n-odd} \frac{2}{\pi n} \sin\left(\frac{2\pi n}{H} z\right) \exp\left(-D\frac{4n^2\pi^2}{H^2} t\right). \tag{2.4}$$

Here, $H = 1$ cm is the total depth of the fluid and $D = 1.1 \times 10^{-5}$ cm^2 s^{-1} is the coefficient of diffusion of salt in water. Profiles of the concentration c for different times $t = 0$, 6 and 60 min are depicted in figure 3. We can see that immediately after the filling stops, the initial step-like distribution is smoothed by diffusion. Although the diffusion is very fast initially, when the gradient of concentration is very high it slows down with time such that even after 1 h, the density difference still remains large (typically, one series of experiments was finished within a 1 h period). The value of buoyancy frequency at the interface varies from $N = 9$ s^{-1} immediately after the filling to $N = 4$ s^{-1} after a 1 h period. Thus, the frequency of the internal oscillator in the flow is much lower than the buoyancy frequency such that the system is far from resonance. However, the emission of high-order normal modes is still possible. An estimate of the magnitude of the vertical displacement of the interface gives $\zeta = (2a/T)/N = 0.05$ cm. This value is small enough for the energy loss associated with the emission of the internal waves to be neglected. In fact, the energy loss for the unsteady quasi-two-dimensional flows is small (of the order of a few per cent) even when the stratification

is much weaker and the flow is closer to resonance. It was shown to be the case for colliding vortex dipoles in two-layer fluid (Afanasyev 2003).

The flow was visualized by the pH-indicator thymol blue. The solution of this indicator is of orange–yellow colour in its neutral state and is deep-blue in the basic state. A few drops of the basic solution of the indicator were injected into the upper layer along the axis of motion of the magnet before each experiment. The fluid particles marked by the indicator are clearly visible and of neutral density. Since the water in the upper layer was made slightly acidic, it takes only a few minutes after the experiment for the injected blue fluid to become yellow again owing to diffusive chemical reaction. The flows were recorded using a video camera or a photo camera placed above the container. Geometrical characteristics of the flow were then measured using the individual frames of a video sequence. The horizontal velocity field in the flow was measured using a PIV technique where variational filtering and interpolation were used for post-processing of data. A description of the method and general technique of PIV is given by Fincham & Spedding (1997) while the variational method is described in Afanasyev & Demirov (2005). Videos of the experiments were recorded in plan view using a digital video camera with an array resolution of 1032×1032 pixels. The typical spatial resolution of the images was 35.5 pixels cm^{-1}. The seeding particles were polyamid spheres of mean diameter 50 μm and density $1.03\,\mathrm{g\,cm}^{-3}$. The density of the particles corresponds to a density of water with salt concentration of approximately $37\,\mathrm{g\,l}^{-1}$. A suspension of particles in water of neutral density was introduced into the interface between the layers. Particles were made visible by illuminating the interface with a sheet of light from a 1 W argon ion laser. The light sheet was created by a cylindrical lens. Since the index of refraction of the stratified fluid varies significantly with depth, it was difficult to adjust the light sheet such that the area of the flow was illuminated uniformly. To avoid this problem, the light sheet was made quite thick. However, since the particles were mainly at the interface at their equilibrium density level, the fact that a thick layer of fluid was illuminated did not introduce any additional uncertainties into the PIV procedure.

Our experimental set-up involved a relatively thin two-layer fluid. Although the estimates of different effects which might affect the two-dimensional character of the flow including boundary layers, surface and internal waves, show that the flows can indeed be considered approximately two-dimensional in this system, the ultimate test which would show that the results of the experiments described herein are of more general character and are rig independent, must include a comparison with a well-documented flow. The flow about a circular cylinder is a benchmark flow in fluid dynamics and is a natural choice for the purpose of comparison. We towed two different cylinders of diameter $d = 0.487$ and 0.315 cm when all other parameters (including the towing velocity and the stratification) of the system were similar to those used in our experiments with magnets. Typical regimes including steady wakes and Kármán–Bénard vortex streets (figure 4) were observed in the experiments where the Reynolds number was varied in the range $Re = 40$–180. Frequency of oscillations in the unstable wakes was measured in these experiments. The results are plotted in figure 5 in the form of the Roshko number as a function of the Reynolds number which are defined in a standard manner. The solid line indicates the empirical dependence $Ro = 0.21(Re – 20.5)$ (Tritton 1959). Our experimental results are in good agreement with this dependence which itself represents the results of a large number of classical experiments with circular cylinders. This comparison provides the assurance that the results of our experiments with magnets reported herein are not sensitive to the particular details of the apparatus and can be considered in a more general context.

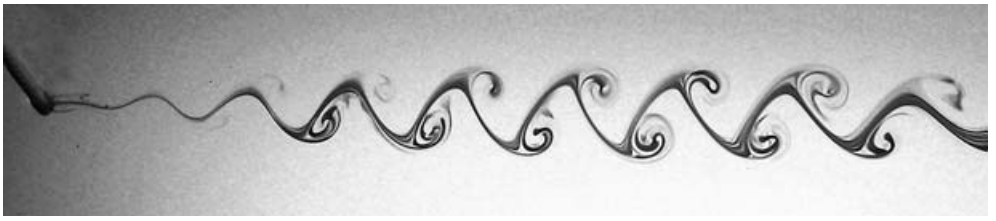

FIGURE 4. Kármán–Bénard vortex street behind a circular cylinder of diameter $d = 0.478$ cm moving with velocity $U = 1.74\,\mathrm{cm\,s^{-1}}$, $Re = 83$.

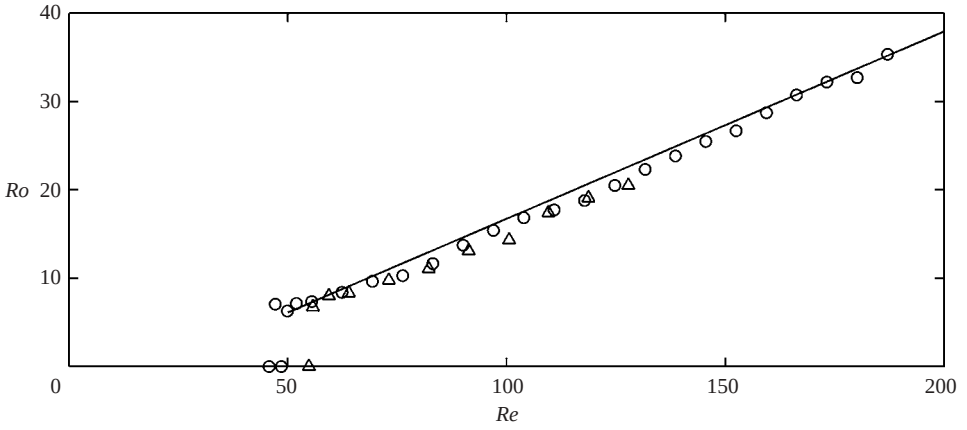

FIGURE 5. The Roshko number versus the Reynolds number for the towed cylinders of diameters $d = 0.478$ (circles) and 0.315 cm (triangles). The solid line shows the dependence (3.7).

3. Experimental results and interpretation

In order to identify different regimes of the flow, a number of experiments were performed where the main control parameters, namely the translation speed of the magnet U and the momentum flux J, have been varied. Figure 6 demonstrates typical images of the flow in the experiments with a single force. When the speed of the magnet was relatively large while the force was relatively weak, the wake behind the magnet was stable and was in the form of a jet (figure 6*a*) flowing in the direction of motion of the force. In this regime, the flow induced by the magnet is completely overwhelmed by the stream and no recirculation occurs under the magnet. For higher values of J, undulations of the jet were observed (figure 6*b*). In some experiments, these undulations develop into a vortex street consisting of an antisymmetric array of vortices (interconnected vortex dipoles) well after the forcing is passed (figure 6*c*). It will be shown later, however, that the initial form of the instability of the jet flow is in fact symmetric in the form of a chain of dipoles moving after one another along the jet axis. For even higher values of J, the formation of a recirculation in the form of a vortex dipole was observed under the magnet and a stable jet behind it (figure 7). Note that the existence of the regimes with the recirculation is in accord with the results of our recent numerical simulations of the flows generated by a moving localized force (Afanasyev & Korabel 2006). The size of the dipole depends on the relative values of J and U. Figure 7 depicts the case when the velocity is relatively low such that the dipole is large compared to the size of the magnet. The centre of the dipole in figure 7 is located at some distance downstream of the centre

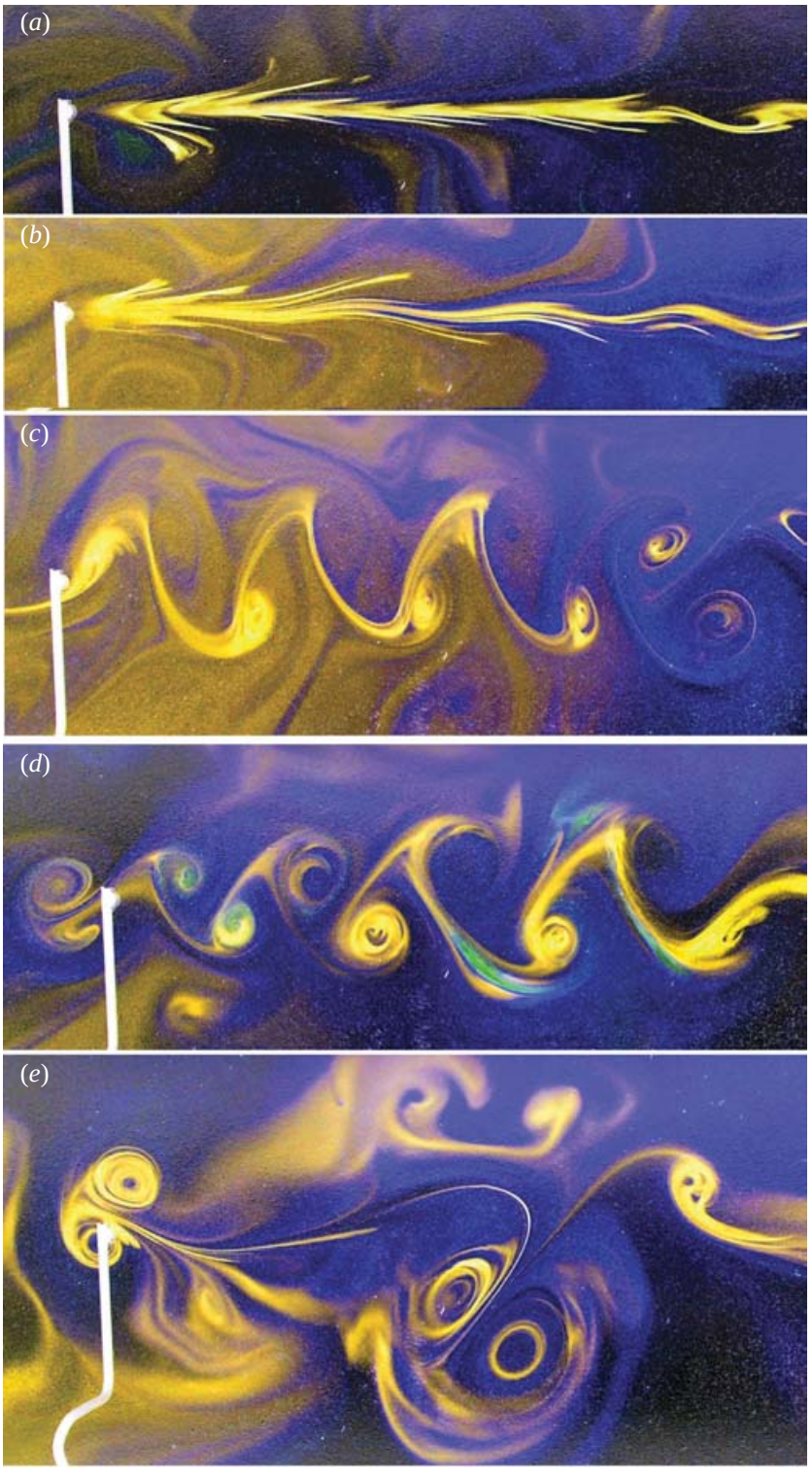

FIGURE 6. For caption see facing page.

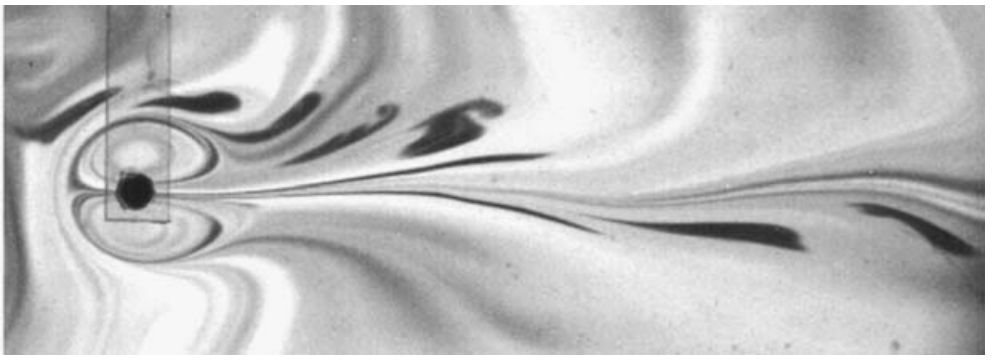

FIGURE 7. Recirculation in the form of a vortex dipole with a trailing wake behind it. The magnet is the black circle at the end of a transparent Plexiglas plate. Experimental parameters: $U = 0.29\,\mathrm{cm\,s^{-1}}$, $J = 0.7\,\mathrm{cm^3\,s^{-2}}$, $\Pi_a = 33$.

of the magnet. If the value of J is further increased, the dipole becomes stronger such that its centre shifts upstream. The dipole does not remain stable, however, and starts shedding vortices. As the dipole loses vorticity of one sign it becomes asymmetric and eventually turns in the direction of rotation of the remaining vortex (figure 8). After a transient stage shown in figure 8, a regular vortex shedding establishes when the dipole disappears, but the vortices of alternating sign are rather generated periodically under the magnet (figure 9). This results in the formation of a typical Kármán–Bénard vortex street in the wake similar to that shown in figure 6(*d*). When the forcing is increased even further, the nonlinearity of the flow increases to such an extent that the forcing produces strong compact vortex dipoles which then eject in different directions quasi-periodically without forming an organized vortex street (figure 6*e*).

Further insight into the dynamics of the unstable wakes can be provided by PIV measurements. Figure 10 demonstrates the velocity and vorticity fields for three different regimes of the flow. A stable jet is shown in figure 10(*a*) while figure 10(*b*) shows a typical form of instability of the jet. This particular regime of instability corresponds to that shown in figure 6(*a*). The unstable flow is symmetric with respect to the axis of the jet and is in the form of dipoles where the vorticity of the jet is concentrated. The dipoles propagate in the same direction as that of the jet. Finally, the regime of the Kármán–Bénard vortex street where an antisymmetric array of vortices is shed from the vortex dipole is shown in figure 10(*c*). The measurements of the velocity field in the stable jet (figure 10*a*) allow us to perform a comparison with theoretical results. The vorticity and velocity fields in the jet generated by a translating point force in a viscous fluid were previously found in the Oseen approximation (Afanasyev 2004). The x and y velocity components, can be obtained

FIGURE 6. Top view images of the flow generated by a single magnet for different regimes: (*a*) jet flow in the wake of the moving magnet, (*b*) weakly unstable jet, (*c*) further development of the unstable jet when the magnet is stopped, (*d*) Kármán–Bénard vortex street (the magnet is stopped shortly before the picture is taken, the dipole in front of the magnet is generated after the magnet was stopped), (*e*) unstable wake in the form of vortex dipoles. The magnet is located at the end of a support rod. Diffused yellow colour in the background remained from the previous experiments. Experimental parameters: (*a*) $U = 1.45\,\mathrm{cm\,s^{-1}}$, $J = 0.8\,\mathrm{cm^3\,s^{-2}}$, $\Pi_a = 2.5$; (*b*) $U = 0.87\,\mathrm{cm\,s^{-1}}$, $J = 0.48\,\mathrm{cm^3\,s^{-2}}$, $\Pi_a = 2.5$; (*c*) $U = 1.74\,\mathrm{cm\,s^{-1}}$, $J = 1.6\,\mathrm{cm^3\,s^{-2}}$, $\Pi_a = 2.1$; (*d*) $U = 1.16\,\mathrm{cm\,s^{-1}}$, $J = 1.1\,\mathrm{cm^3\,s^{-2}}$, $\Pi_a = 3.3$; (*e*) $U = 0.87\,\mathrm{cm\,s^{-1}}$, $J = 1.35\,\mathrm{cm^3\,s^{-2}}$, $\Pi_a = 7.1$.

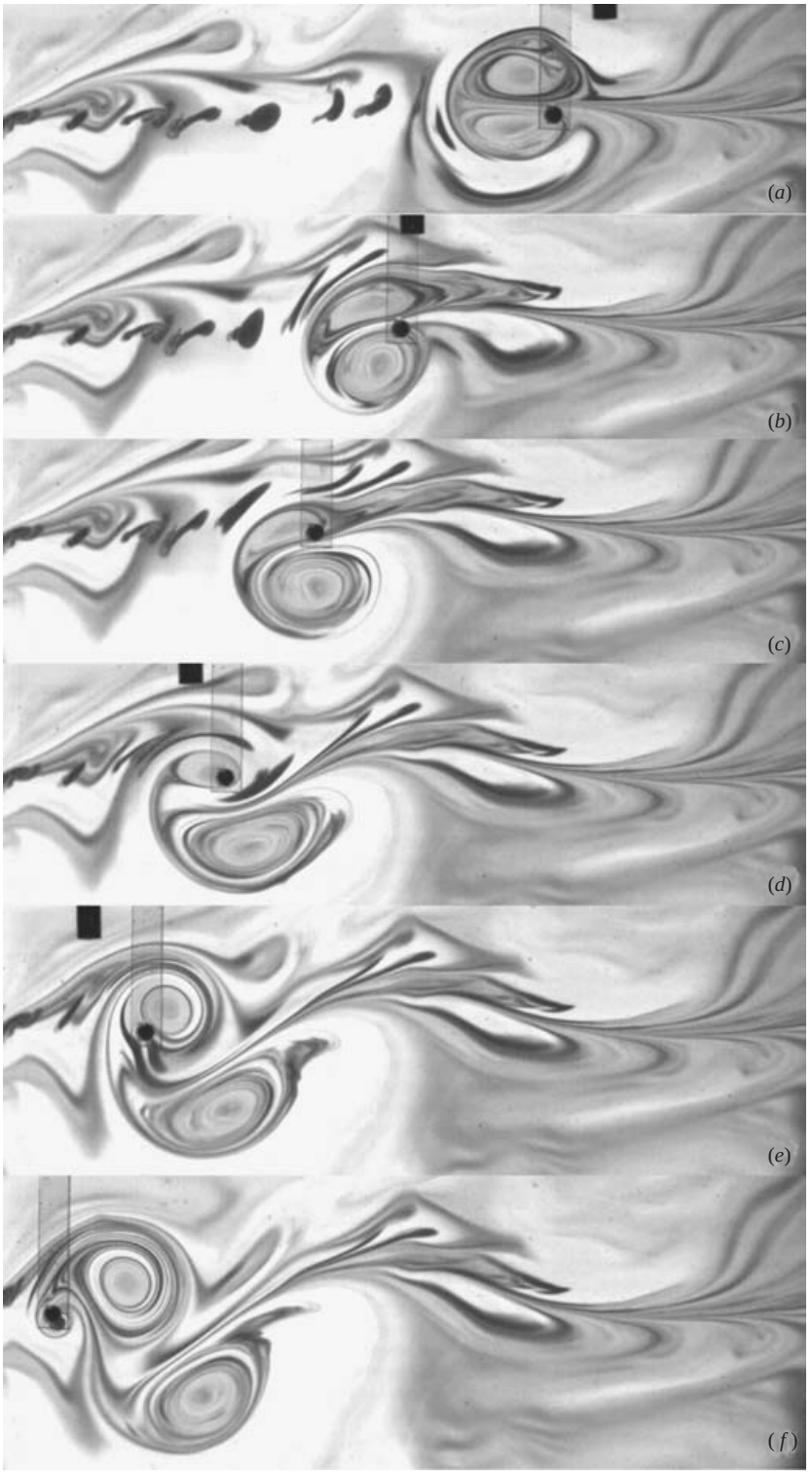

FIGURE 8. Sequence of video frames showing transient vortex shedding by an unstable dipole. Experimental parameters: $U = 0.29\,\mathrm{cm\,s^{-1}}$, $J = 1.7\,\mathrm{cm^3\,s^{-2}}$, $\Pi_a = 81$.

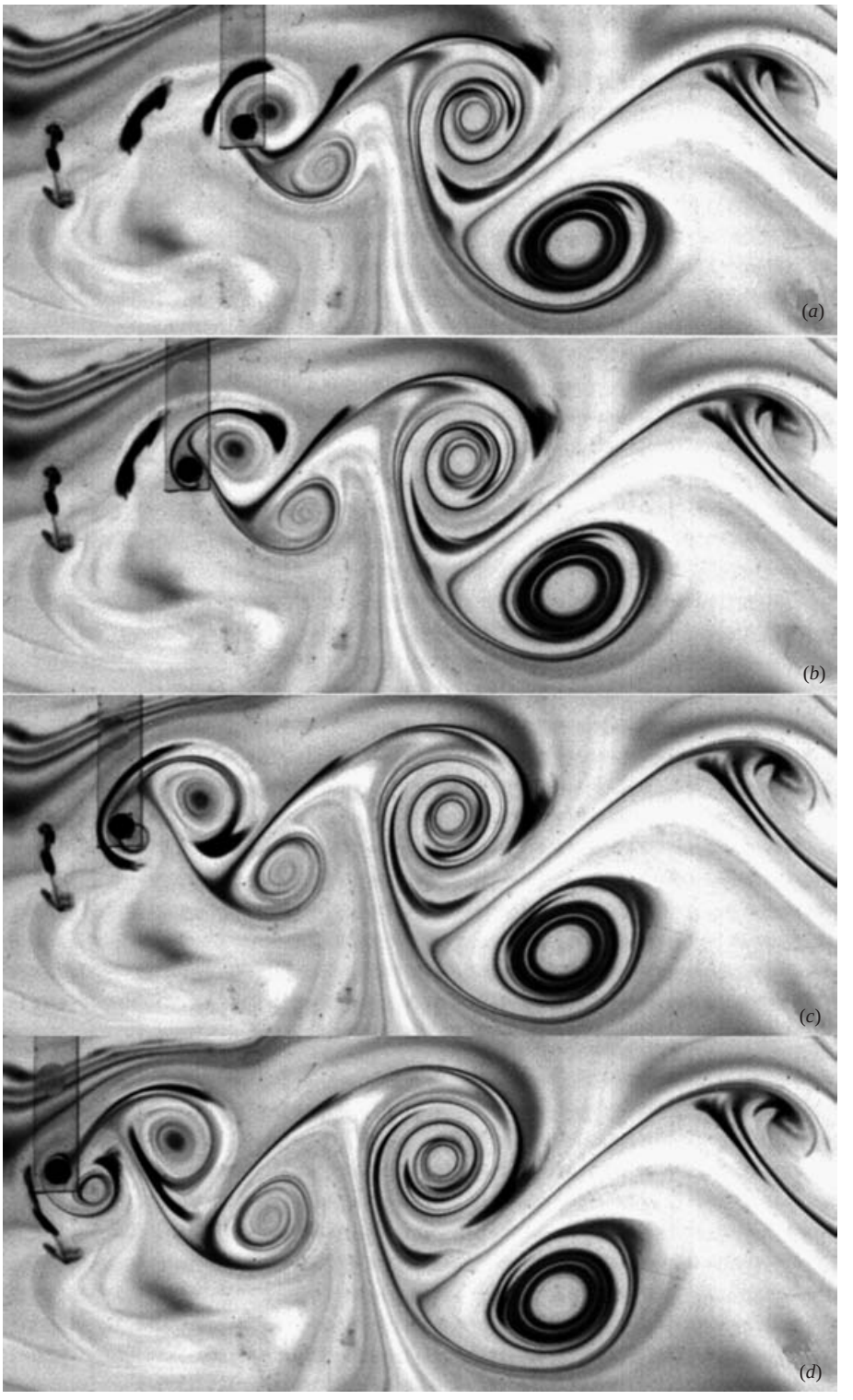

FIGURE 9. Sequence of video frames showing different phases of a regular vortex-shedding regime. The regular regime establishes after the transient regime shown in figure 8. In this regime, a dipole does not form under the magnet, but rather single vortices of alternating rotational sense are formed and shed. Experimental parameters: $U = 0.58\,\mathrm{cm\,s^{-1}}$, $J = 4.25\,\mathrm{cm^3\,s^{-2}}$, $\Pi_a = 51$.

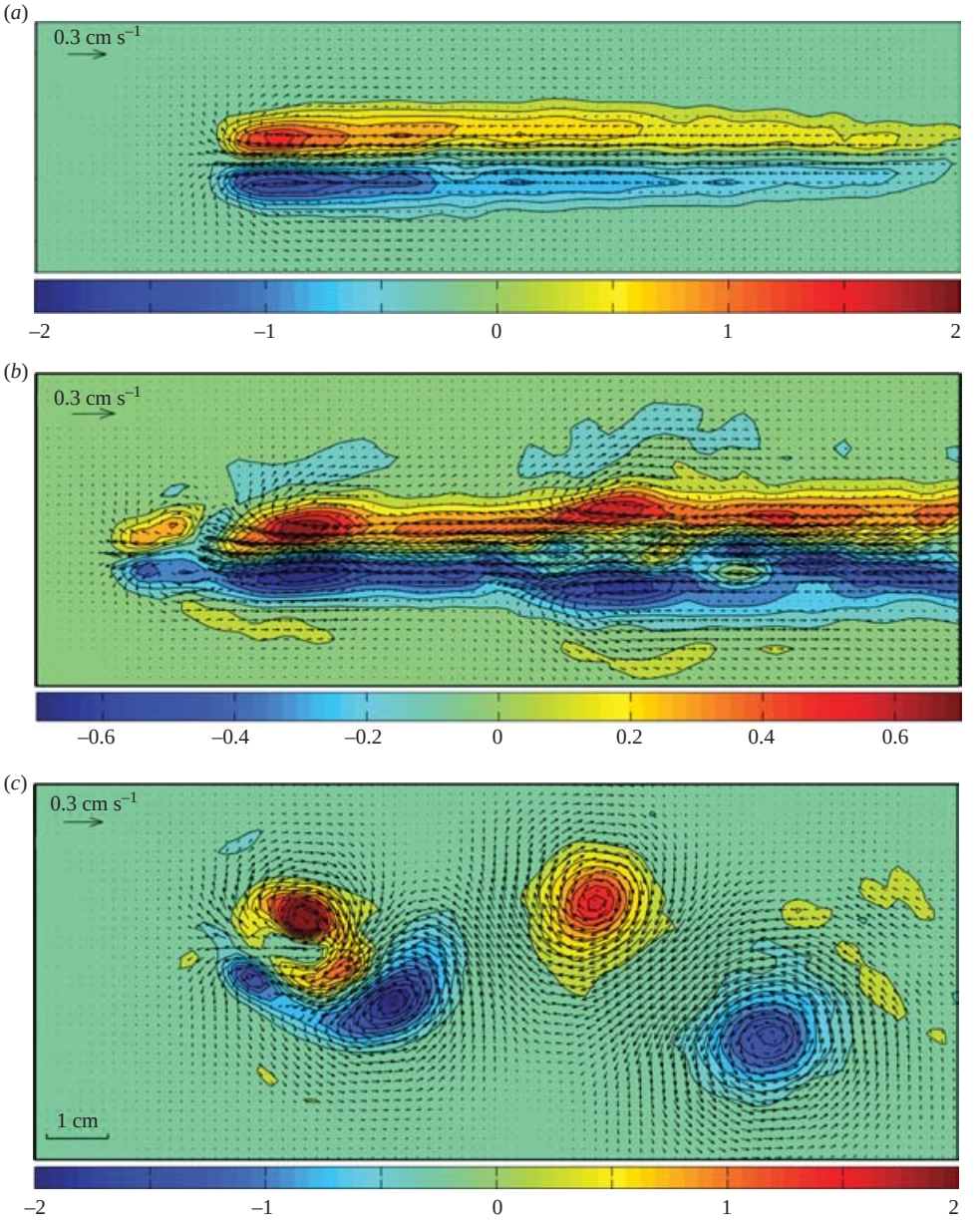

FIGURE 10. Vorticity (colour) and velocity (arrows) fields measured in the experiments with a single magnet for different regimes of the flow: (*a*) stable wake, $U = 1.45\,\mathrm{cm\,s^{-1}}$, $J = 0.54\,\mathrm{cm^3\,s^{-2}}$, $\Pi_a = 1.0$; (*b*) weakly unstable jet where the symmetric 'varicose' instability is observed in the form of a chain of vortex dipoles, $U = 1.6\,\mathrm{cm\,s^{-1}}$, $J = 1.1\,\mathrm{cm^3\,s^{-2}}$, $\Pi_a = 1.7$ and (*c*) Kármán–Bénard vortex street, $U = 0.58\,\mathrm{cm\,s^{-1}}$, $J = 0.54\,\mathrm{cm^3\,s^{-2}}$, $\Pi_a = 6.4$. The colour bars show the vorticity scale in $\mathrm{s^{-1}}$.

by differentiation of the streamfunction of the flow:

$$\psi(x, y) = -\frac{Jy}{2\pi}\int_0^\infty \frac{1 - \exp\left[-\dfrac{x'^2 + y^2}{4\nu\zeta}\right]}{x'^2 + y^2}\,\mathrm{d}\zeta, \tag{3.1}$$

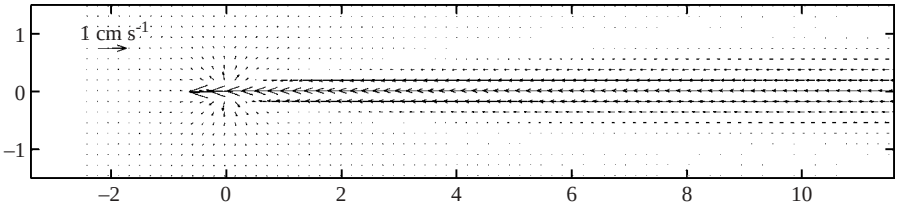

FIGURE 11. Velocity field for the flow induced by a moving point force calculated from the theoretical solution (2). Scale in cm.

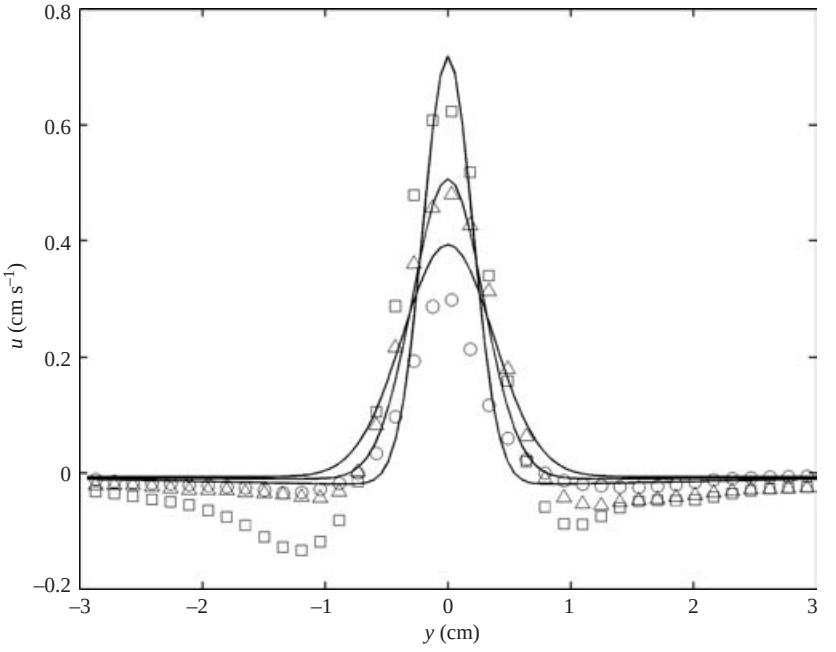

FIGURE 12. Profiles of the x-component of velocity in the jet at three different distances ($x = 3$, 6 and 10 cm) from the origin where the forcing is located. Solid lines represent the theoretical solution (2) while symbols show the results of the PIV measurements (same as in figure 3a).

where $x' = x - U\zeta$. The velocity vectors are shown in figure 11, which can be compared with the velocity field in figure 10(a). The values of the control parameters J and U are the same for theory and the experiment. Comparison shows some similarities as well as differences. In order to compare this data in a quantitative manner we plotted the profiles of the x-component of velocity, u, for three different distances from the origin (where the forcing is located). The experimental data (the key for symbols is given in table 1) and theory (solid lines) in figure 12 demonstrate that the width of the jet remains approximately constant in the experiments, whereas, according to theory, it must increase with the distance from the origin. The most important discrepancy between the theory and the experiment is the significant return flow at the sides of the jet which is observed in the experiment. The return flow predicted by theory is very weak. This discrepancy is due the approximate nature of the solution which does not take into account the advective transport of vorticity by the flow or the effect of the finite size of the forcing area. The lateral motion of fluid towards the axis of the jet can be an important factor by providing transport

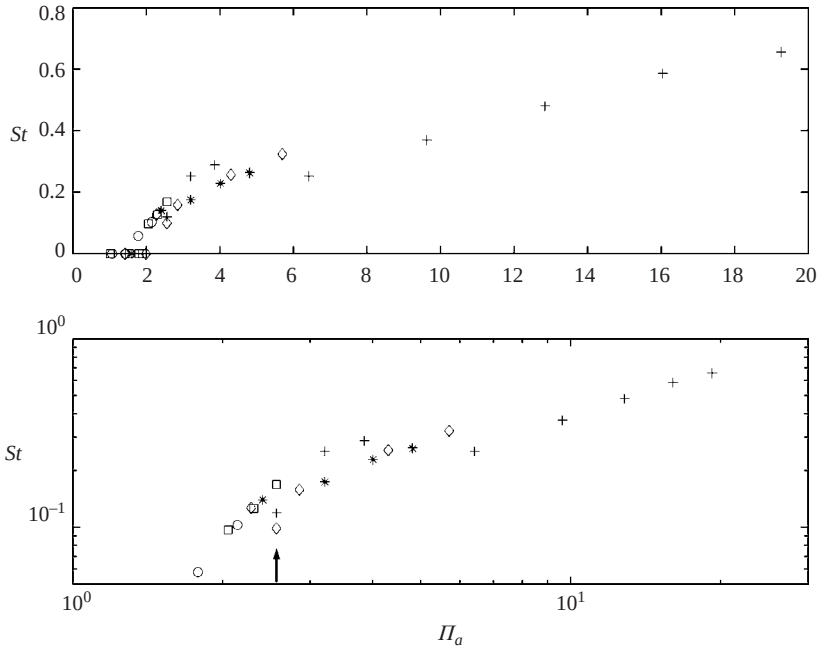

FIGURE 13. The Strouhal number versus Π_a for five series of experiments with a single magnet in linear and logarithmic scale. The legend for symbols is given in table 1.

which compensates the effect of viscous diffusion of momentum directed away from the axis. This may explain why the jet does not widen in the manner predicted by the solution. Another significant factor may be the size of the forcing area. While theory is developed in the assumption of a point force, the effect of the size of the forcing area, a, can be important for the dynamics of the stable jet. Our previous numerical simulations (Afanasyev & Korabel 2004) of jets and vortex dipoles generated by a localized forcing in initially quiescent fluid demonstrated that when a was small enough, the comparison of results of numerical simulations with theory was quite good. The flow did not form concentrated vortices in that case. In contrast, for larger a, the compact vortex dipole was formed at the front of the developing jet. The dipole propagated faster than was predicted by theory because the theory neglected the effect of self-induction of vortices. This dipole also remained a compact structure during its evolution. The effect of the finite size of the forcing area (or rather the effect of the corresponding dimensionless parameter which includes a) will be also discussed here in the context of the dynamics of the vortex shedding for unstable flows.

The wavelength of the perturbations, λ was measured in our experiments for different regimes of the flow. The wavelength was defined as a distance between the peaks in the meandering jet such as the one in figure 6(b) or the distance between the vortices of the same sign in the vortex street (figure 6d). The frequency of the perturbations can then be introduced as $f = U/\lambda$. In order to understand better the behaviour of f for different values of the control parameters involved in the problem, it is useful to perform first a simple dimensional analysis. Frequency f depends on a set of four dimensional quantities including kinematic viscosity ν, velocity U, the amplitude of forcing J and the size of the region where the force is applied, a.

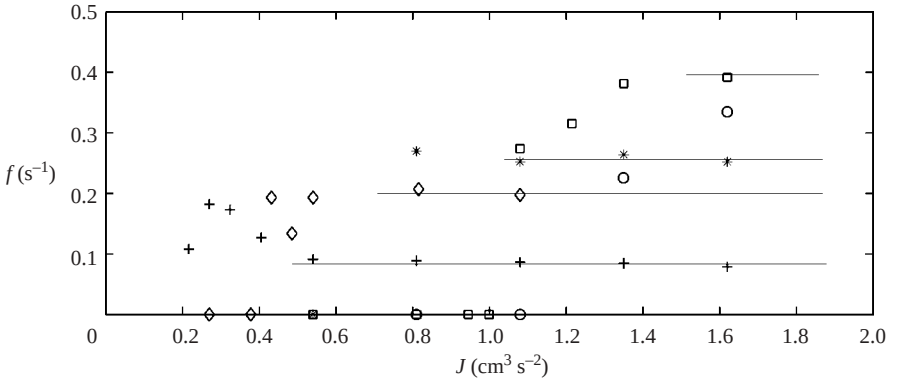

FIGURE 14. Frequency of vortex shedding for different values of the forcing magnitude. Solid lines indicate the asymptotic values of frequency for large J in the experiments with different U. Symbols are the same as those in figure 11.

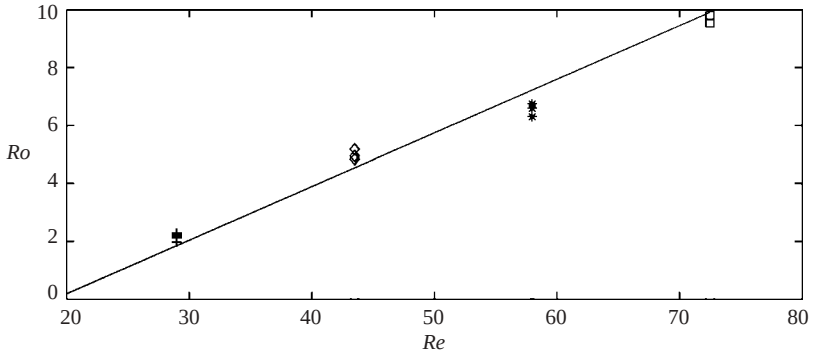

FIGURE 15. The Roshko number versus the Reynolds number for the flows where the Kármán–Bénard vortex street was formed.

Dimensional analysis then gives

$$f = \frac{U^3}{J}\Phi\left(\frac{J}{\nu U}, \frac{J}{aU^2}\right), \tag{3.2}$$

where Φ is an unknown function of two dimensionless arguments. The first argument $\Pi_\nu = J/\nu U$ of the function Φ represents the effect of viscosity while the second argument $\Pi_a = J/aU^2$ represents the effect of the finite size of the source. Π_a can also be interpreted as the ratio of the momentum flux delivered by the forcing to the momentum per unit time transported by the stream through the cross-section of the forcing area. Relation (3.2) can then be rewritten in the dimensionless form as follows:

$$St = \Phi(\Pi_\nu, \Pi_a), \tag{3.3}$$

where $St = fJ/U^3$ is an analogue of the Strouhal number (dimensionless frequency) defined for the flow around a cylinder as $St_c = fd/U$, where d is the diameter of the cylinder. Note that the force applied by the cylinder on the fluid is not an independent parameter, but rather depends on the control parameters of the flow $J = C_D dU^2/2$, where C_D is the drag coefficient dependent on the Reynolds number of the flow. Thus, the Strouhal number introduced here is related to that for the cylinder as

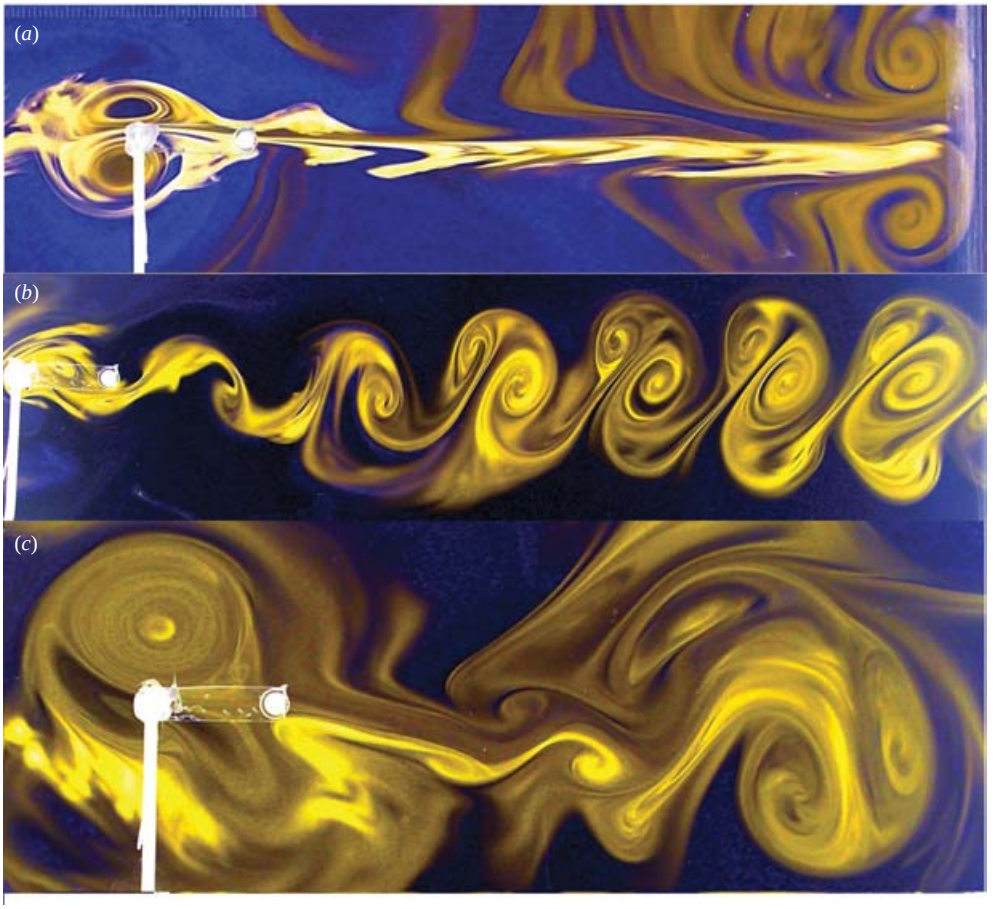

FIGURE 16. Images of the flow generated by two magnets for different regimes: (*a*) stable regime where a dipole is formed under the front magnet and a jet is generated by the rear magnet which provides the thrust. The starting vortex dipole generated when the forcing was started is visible in the left hand side of the picture; (*b*) inverted Kármán–Bénard vortex street (the axes of the interconnected dipoles in the wake are inclined slightly towards the direction opposite to that of the motion of the magnets which is especially clear in the near wake); (*c*) highly unstable irregular wake. Top view. Experimental parameters: (*a*) $U = 0.58\,\mathrm{cm\,s^{-1}}$, $J = 0.7\,\mathrm{cm^3\,s^{-2}}$, $\Pi_a = 8.3$; (*b*) $U = 0.87\,\mathrm{cm\,s^{-1}}$, $J = 2.0\,\mathrm{cm^3\,s^{-2}}$, $\Pi_a = 11$ and (*c*) $U = 0.29\,\mathrm{cm\,s^{-1}}$, $J = 2.0\,\mathrm{cm^3\,s^{-2}}$, $\Pi_a = 95$.

$St = C_D St_c/2$. The Strouhal number is plotted in figure 13 as a function of Π_a for five series of experiments. In each series, the value of velocity U was fixed while the magnitude of the forcing J was varied (table 1). The graph shows that transition between the regimes of the stable jet ($f = 0$) and unstable meandering jet occurs at $\Pi_a \approx 2$. The second transition from the meandering jet to the Kármán–Bénard vortex streets is not immediately obvious from the data, but it can be identified from the analysis of the images of the flow. The analysis shows that the transition occurs at $\Pi_a \approx 2.5$. There is a small step in the graph (marked by an arrow in figure 13) at this value of Π_a. The data points in the St versus Π_a graph corresponds to different values of Π_v. However, the data collapse well onto a single curve for $\Pi_a < 2.5$, indicating negligible dependence of the function $St = \Phi(\Pi_v, \Pi_a)$ on its first argument. The data

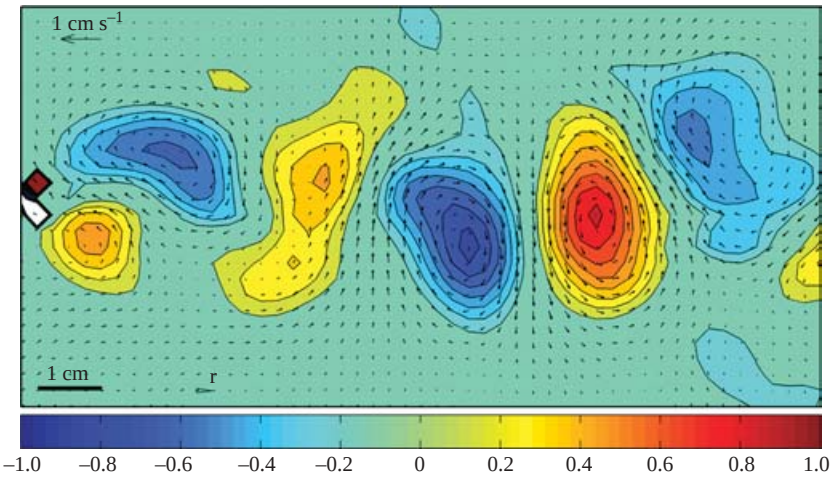

FIGURE 17. Vorticity (colour) and velocity (arrows) fields measured in the experiment with two magnets: $U = 0.87\,\mathrm{cm\,s^{-1}}$, $J = 0.81\,\mathrm{cm^3\,s^{-2}}$, $\Pi_a = 4.3$. The colour bar shows the vorticity scale in $\mathrm{s^{-1}}$.

points in this range of Π_a are characterized by relatively large values of velocity. The scatter in the data for the larger values of Π_a, however, is more significant, implying that the dependence on Π_v must be taken into account. To clarify this dependence, let us return to the dimensional variables. A plot of frequency as a function of J for the series of experiments with different velocity U (figure 14) demonstrates that the frequency remains approximately constant with J when the flow is in the vortex street regime (J is sufficiently large). The values of f in this regime for four series of experiments (different U) are indicated by straight lines in figure 14. For the fifth series (circles) which correspond to the largest U, the forcing was not strong enough for the flow to reach the vortex street regime. The constant values of f can be plotted then as a function of U. However, this can be done also in terms of new dimensionless parameters, namely the Roshko number and the Reynolds number defined as follows:

$$Ro = \frac{fd^2}{\nu},$$

$$Re = \frac{Ud}{\nu}.$$

Here, $d = 2a$ is the diameter of the forcing region. These numbers are used to describe the flow around a circular cylinder, which is one of the well-studied flows in fluid mechanics (e.g. Zdravkovich 1997). We can therefore establish a similarity between the flow generated by localized forcing and the flow around the cylinder. The plot of Ro versus Re where only the data points for the flow in the established vortex street regime are considered, is shown in figure 15. A linear fit gives the dependence of the form

$$Ro = 0.18(Re - 18). \tag{3.4}$$

This dependence is very close to that of the flow around a cylinder. A number of such dependences have been offered in literature during a period of more than 100 years.

Some well-known examples include:

$$Ro = 0.195(Re - 20.1) \quad \text{(Rayleigh 1879)}, \tag{3.5}$$

$$Ro = 0.212(Re - 21.2) \quad \text{(Roshko 1952)}, \tag{3.6}$$

$$Ro = 0.21(Re - 20.5) \quad \text{(Tritton 1959)}. \tag{3.7}$$

Note, that in (3.4), the diameter of the magnet is taken as an estimate of the effective size of the forcing region. This might account for the small discrepancy between the numerical values of coefficients in (3.4) and those in the relations for the cylinder. Thus, the dynamics of the flow in the regime when the Kármán–Bénard vortex street forms in the wake is similar to that of the flow around a cylinder for moderate values of the Reynolds number ($40 < Re < 150$).

Consider now the results of the experiments where two magnets moving over the surface of the water applied forces of equal magnitude, but of opposite direction. A stable regime is characterized by the formation of a jet (not shown here) for relatively low values of J. For higher values of the magnitude of forcing, a meandering of the jet similar to that in the experiments with a single magnet, was observed. Figure 16(a) demonstrates a typical view of the flow in a regime when the magnet at the front generates a dipole stationary in the oncoming stream of velocity U while the magnet at the rear generates a jet flow in the direction opposite to that of the translation of the magnets. A starting vortex dipole can also be seen at the extreme right in figure 16(a). Figure 16(b) demonstrates the flow for even higher values of the magnitude of forcing where a regular vortex street is formed in the wake. This vortex street is visually different from the Kármán–Bénard vortex streets observed in the experiments with a single magnet, and can be referred to as an inverted Kármán–Bénard vortex street. The inverted Kármán–Bénard vortex streets were observed in the wakes of thrust-generating objects such as swimming fish (e.g. Triantafyllou & Triantafyllou 1995; Barrett *et al.* 1999; Triantafyllou, Triantafyllou & Yue 2000; Vandenberghe, Zhang & Childress 2004). While the Kármán–Bénard vortex street consists of interconnected dipoles, the vortex street for the force doublet can be characterized as an array of interconnected vortex quadrupoles. Each of the quadrupoles consists of two dipoles. Since the prototype flow generated by a stationary localized force is a vortex dipole while the flow generated by a stationary force doublet is a vortex quadrupole (e.g. Voropayev & Afanasyev 1994) the arrangement of vortices in the vortex streets correspond to the generic structure of the forcing. A typical vorticity field in the vortex street in the zero momentum wake is shown in figure 17. In the far wake, elongated vortices of alternating sign form an array along the x-axis. This is clearly different from the vortex street in the wake generated by a single force where vortices form an alternating pattern (figure 4d). Figure 16(c) illustrates the regime of the flow when the forcing is rather strong while the translation velocity is relatively low. The front magnet generates large-scale unsteady dipoles while the rear magnet generates an unstable jet. The overall appearance of the flow is irregular in this regime.

The wavelength of the perturbations were measured in the experiments with a force doublet when the wake was unstable in the form of either a meandering jet or the regular vortex street. The dependence of the Strouhal number on the parameter Π_a (figure 18) is, in general, similar to that for the single force (figure 13). The value of Π_a where the transition to instability takes place is approximately $\Pi_a = 2$ and is similar to that for the single force. Note that in the problem with a force doublet, there is one additional dimensional parameter, namely the distance δ between the magnets. However, in our present investigation this distance was fixed, $\delta = 3$ cm.

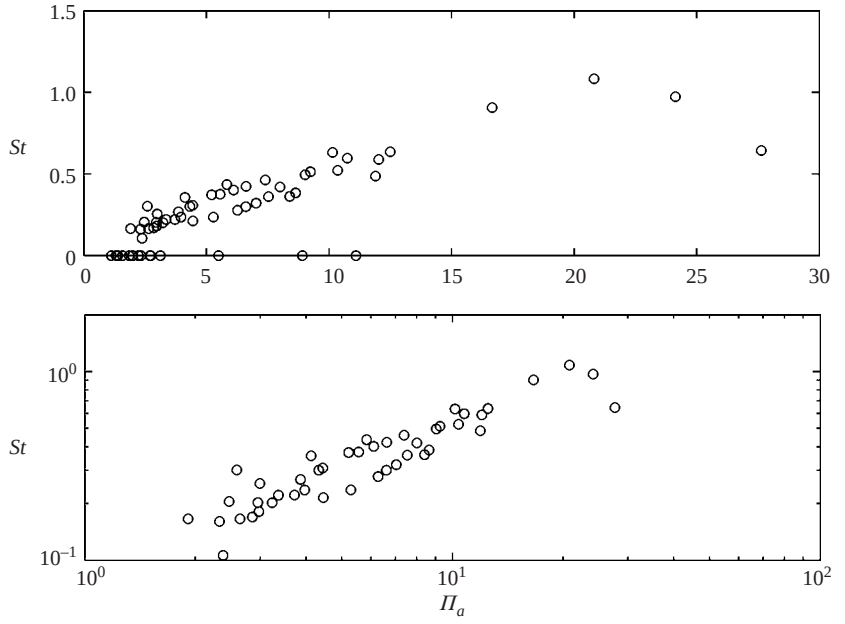

FIGURE 18. The Strouhal number versus Π_a for all series of experiments with two magnets in linear and logarithmic scale.

The dependence of the flow characteristics on this parameter is a subject of further investigations.

4. Discussion

The results of laboratory experiments reported in this paper provide a description of the regimes of the flow generated by a moving 'virtual' bluff body in quasi-two-dimensional geometry. The regimes of the wake for the experiments with a single force simulating the towed body include the steady jet carrying momentum, the unsteady meandering jet where the initial instability is symmetric in the form of a chain of vortex dipoles, the regular Kármán–Bénard vortex street and finally the irregular ejection of vortex dipoles. The approach proposed in this article allows us to look at the initial stages of formation of vortices induced by a forcing and their subsequent shedding. An analogy with a canonical flow around a circular cylinder can again be established here for the case of the meandering jet. Jeon & Gharib (2004) demonstrated that an impulsively started cylinder sheds vorticity in a symmetric manner in the form of a dipole. The vortices then undergo a transformation into an antisymmetric pattern forming a Kármán–Bénard vortex street. The authors speculated that the process of shedding of vorticity from the cylinder is analogous to the process of the formation of vortex rings (in the axisymmetric case) by a stroke of a piston inside a nozzle. The vortex rings do not grow indefinitely according to Gharib, Rambod & Shariff (1998), but have some characteristic formation time equal approximately to the time it takes a piston to travel four diameters of the nozzle. Jeon & Gharib (2004) then extended this result to the flow around a cylinder, demonstrating that the cylinder travels four diameters before the vortex (dipole) is shed. In our previous studies of starting vortex dipoles (Afanasyev & Korabel 2004) we showed that a starting jet forms a dipole at its front which detaches to some extent from the trailing jet when the size of the region

where the forcing was applied was large enough. To establish whether a formation time similar to that for vortex rings exists for starting vortex dipoles generated by a forcing of finite extent, further investigations are necessary. These would provide a more direct analogy with the cylinder flows because of the two-dimensionality of the flow. Note, that the theory of starting dipoles developed previously by different authors (Cantwell 1986; Afanasyev & Voropayev 1989; Voropayev, Afanasyev & Filippov 1991) was based on the notion of a point force obtained in the limit of $a \to 0$. In this context, the importance of a finite size, a, of the forcing region in our experiments should be emphasized. We may think that the formation of vortex streets is still possible in the limit of a point force when $a \to 0$; however, our experiments demonstrate that for very large values of Π_a which correspond to small a, the flows become irregular such that the large-scale vortex dipoles are ejected from the forcing region in different directions. Thus, the finite size of the forcing region (or the size of the body) is a necessary condition for the formation of vortex streets.

The behaviour of the dimensionless frequency of vortex shedding exhibits dependence on the parameter Π_a and negligible dependence on the parameter Π_ν which includes the kinematic viscosity, for relatively high values of the speed U. In the regime of the vortex street, however, when U is smaller and J is larger, the dependence on viscosity becomes significant. This dependence can be expressed in the form of the linear relation between the Roshko number and the Reynolds number of the flow in direct analogy to the relation for the flow around a circular cylinder.

The results of experiments with the force doublet which simulates the self-propelled body were different from those using a single force. The pattern of the vortices behind the force doublet exhibited the inverted Kármán–Bénard vortex street. This pattern consisted of interconnected vortex quadrupoles, which is consistent with the generic structure of forcing. The far wake transforms eventually into an array of vortices of alternating sign located along the x-axis.

The research reported in this paper has been supported by the Natural Sciences and Engineering Research Council of Canada under grants 300805-04 and 227192-04. The authors are grateful to J. Wells for help in conducting the experiments.

REFERENCES

Afanasyev, Y. D. 2003 Spontaneous emission of gravity waves by interacting vortex dipoles in a stratified fluid: laboratory experiments. *Geophys. Astrophys. Fluid Dyn.* **97**, 79–95.

Afanasyev, Y. D. 2004 Wakes behind towed and self-propelled bodies: asymptotic theory. *Phys. Fluids* **16**, 3235–3238.

Afanasyev, Y. D. & Demirov, E. K. 2005 A variational filtration and interpolation technique for PIV employing fluid dynamical constraints. *Exps. Fluids* DOI 10.1007/s00348-005-0017-5.

Afanasyev, Y. D. & Filippov, I. A. 1995 Formation of a vortex street behind an oscillating cylinder. *Fluid Dyn.* **30**, 40–44.

Afanasyev, Y. D. & Korabel, V. N. 2004 Starting vortex dipoles in a viscous fluid: asymptotic theory, numerical simulations and laboratory experiments. *Phys Fluids* **16**, 3850–3858.

Afanasyev, Y. D. & Korabel, V. N. 2006 Wakes and vortex streets behind a localized force: numerical simulations of a virtual bluff body. *Phys. Fluids* (submitted).

Afanasyev, Y. D. & Voropayev, S. I. 1989 On the spiral structure of the mushroom-like currents in the ocean. *Dokl. Akad. Nauk SSSR* **308**, 179–183.

Barrett, D. S., Triantafyllou, M. S., Yue, D. K. P., Grosenbaugh, M. A. & Wolfgang, M. J. 1999 Drag reduction in fish-like locomotion. *J. Fluid Mech.* **392**, 183–212.

Batchelor, G. K. 1967 *An Introduction to Fluid Dynamics*. Cambridge University Press.

Cantwell, B. J. 1986 Viscous starting jets. *J. Fluid Mech.* **173**, 159–189.

Chasnov, J. R. 1997 On the decay of two-dimensional homogeneous turbulence. *Phys. Fluids.* **9**, 171–180.

Danilov, S., Dolzhanskii, F. V., Dovzhenko, V. A. & Krymov, V. A. 2002 Experiments on free decay of quasi-two-dimensional turbulent flows. *Phys. Rev.* E **65**, 036316-1.

Fincham, A. & Spedding, G. 1997 Low cost, high resolution DPIV for measurement of turbulent fluid flow. *Exps. Fluids* **23**, 449–454.

Gharib, M., Rambod, E. & Shariff, K. 1998 A universal time scale for vortex ring formation. *J. Fluid Mech.* **360**, 121–140.

Jeon, D. & Gharib, M. 2004 On the relationship between the vortex formation process and cylinder wake vortex patterns. *J. Fluid Mech.* **519**, 161–181.

Martin, B. K., Wu, X. L., Goldburg, W. I. & Rutgers, M. A. 1998 Spectra of decaying turbulence in a soap film. *Phys. Rev. Lett.* **80**, 3964–3967.

Paret, J., Marteau, D., Paireau, O. & Tabeling, P. 1997 Are flows electromagnetically forced in thin stratified layers two dimensional. *Phys. Fluids* **9**, 3102–3104.

Rayleigh, Lord 1879 Acoustical observations. *Phil. Mag. ser.* 5, **7**, 149–162.

Roh, S. C. & Park, S. O. 2003 Vortical flow over the free end surface of a finite circular cylinder mounted on a flat plate. *Exps. Fluids* **34**, 63–67.

Roshko, A. 1952 On the development of turbulent wakes from vortex streets. PhD thesis, Calfornia Institute of Technology.

Sumner, D., Heseltine, J. L. & Dansereau, O. J. P. 2004 Wake structure of a finite cylinder of small aspect ratio. *Exps. Fluids* **37**, 720–730.

Triantafyllou, M. S. & Triantafyllou, G. S. 1995 An efficient swimming machine. *Sci. Am.* **272**, 64–70.

Triantafyllou, M. S., Triantafyllou, G. S. & Yue, D. K. P. 2000 Hydrodynamics of fishlike swimming. *Annu. Rev. Fluid Mech.* **32**, 33–53.

Tritton, D. J. 1959 Experiments on the flow past a circular cylinder at low Reynolds numbers. *J. Fluid Mech.* **6**, 547–567.

Vandenberge, N., Zhang, J. & Childress, S. 2004 Symmetry breaking leads to forward flapping flight. *J. Fluid Mech.* **506**, 147–155.

Voropayev, S. I. & Afanasyev, Y. D. 1994 *Vortex Structures in a Stratified Fluid*. Chapman and Hall.

Voropayev, S. I., Afanasyev, Y. D. & Filippov, I. A. 1991 Horizontal jets and vortex dipoles in a stratified fluid. *J. Fluid Mech.* **227**, 543–566.

Voropayev, S. I. & Smirnov, S. A. 2003 Vortex streets generated by a moving momentum source in a stratified fluid. *Phys. Fluids* **15**, 618–624.

Voropayev, S. I., Smirnov, S. A., Filippov, I. A. & Boyer, D. L. 2002 Stratified wakes generated by a 'point' momentum source. *Izv. Acad. Sci. USSR Atmos. Oceanic Phys.* **38**, 402–408.

Wells, J. & Afanasyev, Y. D. 2004 Decaying quasi-two-dimensional turbulence in a rectangular container: laboratory experiments. *Geophys. Astrophys. Fluid Dyn.* **98**, 1–20.

Williamson, C. H. K. & Govardhan, R. 2004 Vortex-induced vibrations. *Annu. Rev. Fluid Mech.* **36**, 413–455.

Zdravkovich, M. M. 1997 *Flow Around Circular Cylinders*. Oxford University Press.